**Prevention and Treatment of Natural Disasters**
http://ojs.ukscip.com/index.php/ptnd

**ARTICLE**

# On the Selection of Wavelet Models in the Simulation of Seismic Accelerograms through Evolutionary Optimization

**Daniela Dalla Chiesa**[1] **Letícia Fleck Fadel Miguel**[2*] **Jorge Daniel Riera**[3]

1. Postgraduate Program in Mechanical Engineering (PROMEC), Federal University of Rio Grande do Sul (UFRGS), Porto Alegre, Brazil
2. Department of Mechanical Engineering (DEMEC), Postgraduate Program in Mechanical Engineering (PROMEC), Postgraduate Program in Civil Engineering (PPGEC), Federal University of Rio Grande do Sul (UFRGS), Porto Alegre, Brazil
3. Department of Civil Engineering (DECIV), Postgraduate Program in Civil Engineering (PPGEC), Federal University of Rio Grande do Sul (UFRGS), Porto Alegre, Brazil

**Received:** 28 December 2021; **Accepted:** 18 February 2022; **Published Online:** 18 May 2022

**Abstract:** A numerical procedure, based on an evolutionary optimization algorithm, has been proposed by the authors for the simultaneous generation of the three components of the seismic ground acceleration. The methodology allows the determination of a train of seismic waves modeled by three different waveforms, for the generation of ground seismic acceleration components. The parameters of each wave, *i.e.*, amplitude, frequency, duration, arrival time and direction, are determined using an evolutionary optimization algorithm. Although no theoretical justification is known by the authors for the generation, at the seismic source, of specific initial waveforms, both in case of fracture or of sliding with friction, waveform acceleration components that satisfy the condition of zero final velocity should in principle be preferred. The latter is a physical restriction that is automatically satisfied by anti-symmetrical functions, thus eliminating the need to correct the baseline of simulated accelerograms. The error offit of simulated accelerograms generated by three different waveforms proposed in the literature was herein determined by comparison with actual seismic records. On that basis, estimations of the expected error of the evolutionary optimization algorithm in engineering applications are presented.

**Keywords:** Seismic waves; Waveforms; Error offit; Three components of ground acceleration; Backtracking search optimization algorithm

## 1. Introduction

A turning point in the description of seismic excitation for purposes of structural analysis consisted of the introduction, around the middle of the 20th century, of the

*Corresponding Author:
Letícia Fleck Fadel Miguel,
Department of Mechanical Engineering (DEMEC), Postgraduate Program in Mechanical Engineering (PROMEC), Postgraduate Program in Civil Engineering (PPGEC), Federal University of Rio Grande do Sul (UFRGS), Porto Alegre, Brazil;
*Email: letffm@ufrgs.br*

DOI: https://doi.org/10.54963/ptnd.v1i1.19

assumption that the ground acceleration may be modeled as a unidimensional random process. The first applications considered the ground motion a stationary white noise (Housner, [1]; Bycroft, [2]). Later, a stationary filtered white noise was employed by Tajimi [3]; Kanai [4] and Clough and Penzien [5]. The first nonstationary stochastic models introduced a deterministic envelope function, employed for instance by Shinozuka and Sato [6]; Iyengar and Iyengar [7] and Amin and Ang [8]. The proposed envelope functions, although able to model the evolution of the ground motion intensity, did not account for a known feature of seismic records, namely the change of the predominant frequency with time.

Bruna and Riera [9] noticed that when passed through thin bandpass filters, acceleration records decomposed in a number of short duration components, which presented the form of a harmonic wave modulated by a pulse. These components were called base functions and employed to simulate seismic acceleration records in an entirely different manner, which allowed the consideration, in the simulation scheme, of relevant features of the event under study, such as epicentral distance, focal depth, rupture area, seismic wave type and rupture velocities. Bruna and Riera [9] and more recently Dalla Chiesa and Miguel [10], focused their attention on the simultaneous generation of the three components (East-West, North-South and Vertical) of ground acceleration at a given location employing for such purpose different approaches.

Note here that the underlined assumption is that the initially called base functions, which look similar to acceleration signals recorded in acoustic emission (AE) tests during the fracture of solids, naturally occur within point-like regions in both fracture and sliding with friction processes, causing in an isotropic, homogeneous medium, spherical wavefronts. Based on these assumptions, Dalla Chiesa *et al.* [11] simulated, employing Morlet's wavelets, the seismic acceleration recorded at seismological stations, as well as at neighboring locations. In this context, Iturrioz and Riera [12] confirm, employing numerical solutions, that P and S waves with the form of various so-called wavelets propagate in homogeneous, isotropic media retaining the pulse shape.

As described by Spanos *et al.* [13], several wavelet functions capable of generating meaningful analyzing bases were developed near the end of the 20th century to best suit several problems in science and engineering related to transient, time-variant, or nonstationary phenomena. However, only after the turn of the century, the approach received considerable attention in seismic applications. Thus, it appears that the base functions previously mentioned may constitute special types of wavelet functions. In this context, the family of generalized harmonic wavelets introduced by Newland [14,15], features the appealing property of nonoverlapping Fourier transforms, which renders the corresponding harmonic wavelet transform an exceptional tool in cases in which enhanced resolution in the frequency domain is important. To increase the time resolution as well, filtered harmonic wavelets were employed later by the same author (Newland, [16]). Spanos *et al.* [13] adopt the filtered harmonic wavelet to model single component accelerograms of four large earthquake events in order to determine the nonlinear response of a high steel building. One of the earliest applications of wavelet developments in Earthquake Engineering was described by Gurley and Kareem [17], who also use the approach in Ocean and Wind Engineering transient process simulations.

Montejo and Suarez [18] employ a simple wavelet-based procedure to identify the natural frequencies of a geotechnical site using a free field acceleration record. It is shown that a zoom-in of the wavelet transform of the acceleration record is sufficient to accurately pinpoint at least the fundamental frequency of the site. Zooming-in is the process of magnifying a selected region of the time-frequency plane in which the wavelet transform coefficients are defined. Amiri *et al.* [19] presented later an evolutionary neural network framework to generate multiple spectrum-compatible artificial earthquake accelerograms (SCAEAs). Learning ability of multi-layer feed-forward (MLFF) neural networks was implemented to develop an inverse mapping from response spectrum to earthquake accelerogram. The proposed method was applied to a sample of 128 Iran recorded earthquakes.

Yamamoto and Baker [20] describe an approach by which the wavelet packet transform can be used to characterize earthquake ground motions and illustrate the potential benefits of such an approach in a variety of earthquake engineering applications. A model is developed that requires 13 parameters to describe a given uni-directional ground motion. These parameters are then related to seismological variables such as earthquake magnitude, distance, and site condition, through regression analysis that captures trends in mean values, standard deviations, and correlations of these parameters observed in recorded strong ground motions from 25 past earthquakes. The resulting regression equations can then be used to predict ground motions for a future earthquake scenario. This model is analogous to widely used empirical ground-mo-

tion prediction equations, usually designated attenuation models, except that it directly predicts acceleration *vs.* time samples rather than only response spectra.

Note that all contributions referenced above describe the use of wavelets to simulate one horizontal component of observed seismic ground motion. In this paper, a numerical procedure, based on an evolutionary optimization algorithm, is used for the simultaneous generation of the three components of the seismic ground acceleration. Estimations of the expected error of the evolutionary optimization algorithm for three waveform types are presented, as well as practical considerations on waveforms selection, based on physical arguments as well as on the error offit of simulated accelerograms.

## 2. Model and Waveforms Examined

### 2.1 Description of the Basic Model

The model employed in the ensuing assessment admits that the accelerations in the three orthogonal directions, *i.e.*, q(, a2(t) and a3(t), at the location of interest consist of a train of body waves originated at the hypocenter of the seismic event. The previous assumption is approximately satisfied when the dimensions of the rupture area are perceptibly smaller than the hypocentral distance $D_{hip}$ and the epicentral distance does not exceed the focal depth. These restrictions may be removed, but increasing the computational and analytical effort, since the contribution of surface waves, herein neglected, would also have to be considered.

Each component of the seismic waves train has different frequency, amplitude, duration and orientation and, when reaching the location of interest on the surface, produces accelerations on each of the orthogonal reference axes, with different times of arrival and different amplitudes, $A_1$, $A_2$, $A_3$, as illustrated in Figure 1.

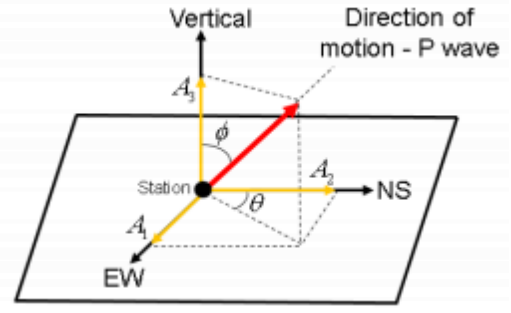


**Figure 1.** Illustration of the propagation direction of a seismic wave.

In Figure 1, the angles $\phi$ and $\theta$ indicate the main orientation of motion. $\phi$ is measured in relation to the vertical axis and θ is measured in relation to the horizontal axis 2.

### 2.2 Seismic Waveforms

To model the acceleration components along the orthogonal directions $i$ ($i$ = 1, 2, 3), the following waveforms are considered:

**Imaginary part of Morlet's wavelets:**

$$a_i(t) = \sum_{j=1}^{N_j} A_{ij} \sin(2\pi f_j t) \exp\left(-t^2/(2s_j^2)\right) u(t - t_{a_j}) \text{ u(tuy-t)}, \quad (1)$$

**Real part of Morlet's wavelets:**

$$a_i(t) = \sum_{j=1}^{N_j} A_{ij} \cos(2\pi f_j t) \exp\left(-t^2/(2s_j^2)\right) u(t - t_{a_j})\, u(t_{b_j} - t), \quad (2)$$

**Bruna and Riera function:**

$$a_i(t) = \sum_{j=1}^{N_j} A_{ij} \sin(2\pi f_j t) \sin\left(\pi t/t_{d_j}\right) u(t - t_{a_j})\, u(t_{b_j} - t). \quad (3)$$

The theory of the complex Morlet wavelet is discussed by Domingues *et al.* [21]. In Equations (1)-(3), $i$ refers to the orthogonal direction of a cartesian coordinate system, $j$ refers to the seismic wave, $N_j$ is the number of waves, u(t) denotes Heaviside's unit step function, $A_{ij}$ is the amplitude of wave $j$ in the direction $i$, $f_j$ is the frequency (in Hz) of each wave $j$, $t$ is the time, $s_j$ the width, $t_{aj}$ the arrival time, $t_{bj}$ the final time of each wave $j$ while , $A_{1j}$= Ajstnstn6, $A_{2j} = A_j \sin\phi_j \cos\theta_j$, and $A_{3j} = A_j \cos\phi_j$ are the orthogonal projections of the amplitude of wave $j$, in the three directions, as illustrated in Figure 1. Notice that $t_{bj} = t_{aj} + t_{dj}$ and $t_{dj} = n_j/f_j$, in which $t_{dj}$ is the duration and $n_j$ is the number of cycles. Figure 2 illustrates the three acceleration histories modeled by the Equations (1)-(3).

The problem is to find the parameters for each seismic wave that allow the generation of the three ground acceleration components registered in a seismic station. For such purpose, an optimization algorithm is herein employed.

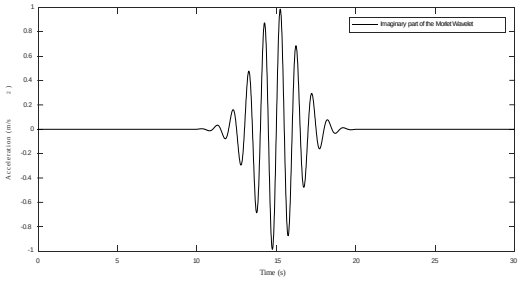

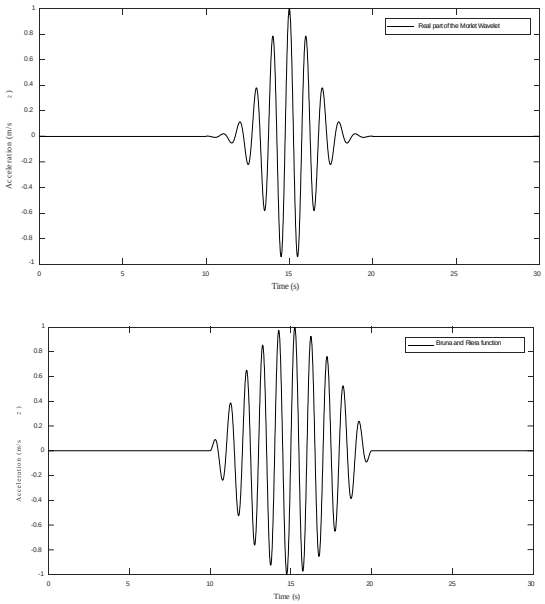


**Figure 2.** Scheme illustrating the three acceleration histories modeled by the Equations (1) - (3). A=1m/s2,ta=10s,tb=20sand td=10s.

## 3. Optimization Procedure

The optimization procedure consists of finding the best design variables $A_j$,$f_j$, $t_{aj}$, $n_j$, $\phi_j$ and $\theta_j$, for each $j$-wave that minimize the objective function,$f_o$:

$$f_o = \sum_{i=1}^{3}\left(F_i \sum_{l=1}^{N_{data}} \left(a_i^R(t_l) - a_i(t_l)\right)^2\right) \quad (4)$$

in which $^*t)$ is the registered accelerogram in the direction $i$, $F_i$ is the weighting factor, and $N_{data}$ is the number of accelerogram data. As the vertical component of the accelerogram usually has smaller amplitudes than the horizontal ones, the weighting factor $F_i$ was determined in order to adjust the orders of magnitude of the 3 components, making them compatible. That is, it was a numerical scheme so that the algorithm optimizes the 3 components of the accelerograms with similar weights.

To determine the best design variables and evaluate the objective function, the Backtracking Search Optimization Algorithm (BSA), proposed by Civicioglu [22] and employed in different optimization problems (*e.g.* Miguel *et al.*, [23,24]), is used. The design variables $A_j$, $f_j$, $n_j$, $\phi_j$ and are generated randomly from a uniform distribution. For the final velocity to be zero, design variables are integer values. The following restrictions are considered for these design variables: $\phi_{min} = 0^o$, $\phi_{max} = 90^o$, $\theta_{min} = az_{S-E} - 90^o$, $\theta_{max} = az_{S-E} + 90^o$, $az_{S-E}$ refers to the earthquake-station azimuth, Amtn=0 , Amx=0.1. The value of$f_{min}$ corresponds to the lowest cut-off frequency of the registered and filtered accelerograms and $f_{max}$ is the highest relevant peak frequency of the three power spectra. The value of $n_{min}$ is estimated in 0 and the value of $n_{max}$ must be calculated in each iteration so that the wave starts and ends within the time interval of the record (to simulate the wave passing through the station). The choice of restrictions was based on plausible parameters of the seismic waves and on previous simulations, in which the authors adjusted the input parameters of the algorithm to obtain the best possible agreement with registeredaccelerograms.

The design variables $t_{aj}$ are generated taking into account the variability regarding the velocities of propagation and the actual path of seismic waves, thus two Gaussian probability distributions, with coefficients of variation of 5% are considered: one for the arrival time of the Primary (P) waves, with average $t_{ap}$, and other for the arrival time of the Secondary (S) waves, with average $t_{as}$. The average arrival times of P and S waves are given, respectively, by:

bw=DW/wp (5)

ts=Ddw/vs (6)

Refractions and reflections are not considered in the arrival time calculation, in which it is also assumed that waves travel along straight lines. The IASP91 velocity model,developed by Kennett and Engdahl [25], is adopted to estimate the average velocities $V_p$ and $V_s$, of the P and S waves, respectively.

### 3.1 Summary of the Methodology

The steps for the proposed procedure for the simultaneous simulation of the three components of seismic accelerograms are next described.

**Selection of the seismic record:** Seismic records (corrected and filtered) containing the three components are selected, based on the assumptions assumed in Section 2.1. The strong motion part of the accelerograms downloaded from the site was selected and a linear interpolation was performed on the registered accelerograms, increasing the time increment to 0.01 s.

**Backtracking search optimization algorithm (BSA):** The optimization process starts with BSA input parameters, *i.e.*, the maximum number of iterations, population size, total number of waves in each accelerogram, minimum value and the maximum value of each design variable, as described in Section 3, are reported to the program and the choice of the waveform, Equations (1)-(3). The

optimization problem consists of finding the best design variables, for each *j*-wave that minimize the objective function described in Equation (4). The process ends after completing the maximum number of iterations.

**Analysis of results:** The results of the three components are analyzed with respect to the earthquake recorded at the station and each waveform: the registered accelerograms and the simulated accelerograms, the registered and simulated pseudo-acceleration spectra, the mean-squared error among the pseudo-acceleration spectra, for the period from 0 s to 2.5 s, the relative error among the peak pseudo-acceleration spectra, the mean-squared error among the accelerogram, the relative error among the peak ground acceleration and the final velocity of the simulatedaccelerograms.

It is important to point out that the proposed methodology allows the determination of a train of seismic waves, which is validated by comparison with the recorded accelerograms and respective response spectra obtained at the seismic station. Later, this same train of seismic waves obtained at the seismic station can be employed to simultaneously generate the three components of seismic accelerograms at other locations on the surface a few kilometers away from the seismic station, as shown by the authors in Dalla Chiesa *et al.* [11].

## 4. Case Studies

To illustrate the methodology and compare the three functions, two seismic events recorded in Italy were selected. The first earthquake occurred on 29 December 2013, at 17:08:43 (event id IT-2013-0019) and was registered at the Piedimonte Matese station (station code PDM). The event, called Caserta, occurred at a depth of approximately 20.40 km (Bollettino Sismico Italiano - INGV-CNT Seismic Bulletin, [26]) and was recorded on a site located at 6.01 km (calculated) of the epicenter.

The second earthquake occurred on 16 January 1981, at 00:37:45 (event id IT-1981-0001) and was registered at the Cairano 4 station (station code CR4). The event, called Southern Italy, was recorded at a depth of approximately 10.5 km (Castello *et al.*, [27]) and was recorded on a site located at 9.46 km (calculated) of the epicenter.

The recorded ground acceleration histories were downloaded from the ESM - Engineering Strong-Motion database (EMS, [28]; Luzi *et al.*, [29]). A portion of the accelerograms downloaded from the site was selected. At the PDM station, the range from 13.4 s to 28 s was selected. In the CR4 station, the interval from 0 s to 17 s was selected. The selection was made because the downloaded accelerograms contain very low or almost zero values of acceleration in the intervals not considered, however, it is important to note that the part that corresponds to the duration of the strong motion of the ground was maintained. The acceleration histories are corrected and filtered. A linear interpolation was performed on the registered accelerograms, increasing the time increment to 0.01 s. Table 1 shows the and parameters (BSA parameters). The parameter indicates the maximum number of iterations. The results, using the three functions, are summarized in the following subsections.

The choice of $N_j$, $A_{min}$, $A_{max}$, $N$ and *maxit* was based on previous simulations (Dalla Chiesa *et al.*, [11]), in which the authors fitted the input parameters of the algorithm in order to obtain the best possible agreement with the recorded accelerogram. The value of $f_{min}$ corresponds to the lowest cutoff frequency of the registered and filtered accelerograms and $f_{max}$ is the highest relevant peak frequency of the three power spectra, a criterion adopted in order to satisfy the three recorded ground acceleration components.

**Table 1.** Parameters used in each simulation.

| Parameters/Station | PDM station | CR4 station |
|---|---|---|
| $N_j$ | 100.00 | 100.00 |
| $A_{min}$ | 0.00 m/s$^2$ | 0.00 m/s$^2$ |
| $A_{max}$ | 0.10 m/s$^2$ | 0.10 m/s$^2$ |
| $f_{min}$ | 0.03 Hz | 0.30 Hz |
| $f_{max}$ | 15.00 Hz | 15.00 Hz |
| $N$ | 30.00 | 30.00 |
| *maxit* | 200,000.00 | 200,000.00 |

### 4.1. Piedimonte Matese Station (2013)

Figures 3-8 present the results of the three components with respect to the earthquake recorded at the PDM station. Figures 3-5 illustrate the registered accelerograms and the simulated accelerograms and Figures 6-8 illustrate the registered and simulated pseudo-acceleration spectra. The vertical bars (in blue) of Figures 3-5 indicate the duration of the strong motion, calculated by the method proposed by Trifunac and Brady [30].

Tables 2-6 show results for the PDM station. Table 2 shows the mean-squared error among the pseudo-acceleration spectra, for the period from 0 s to 2.5 s. Table 3 shows the relative error among the peak pseudo-acceleration spectra. Table 4 shows the mean-squared error among the accelerograms. Table 5 shows the relative error among the peak ground acceleration. Table 6 shows the final velocity of the simulated accelerograms.

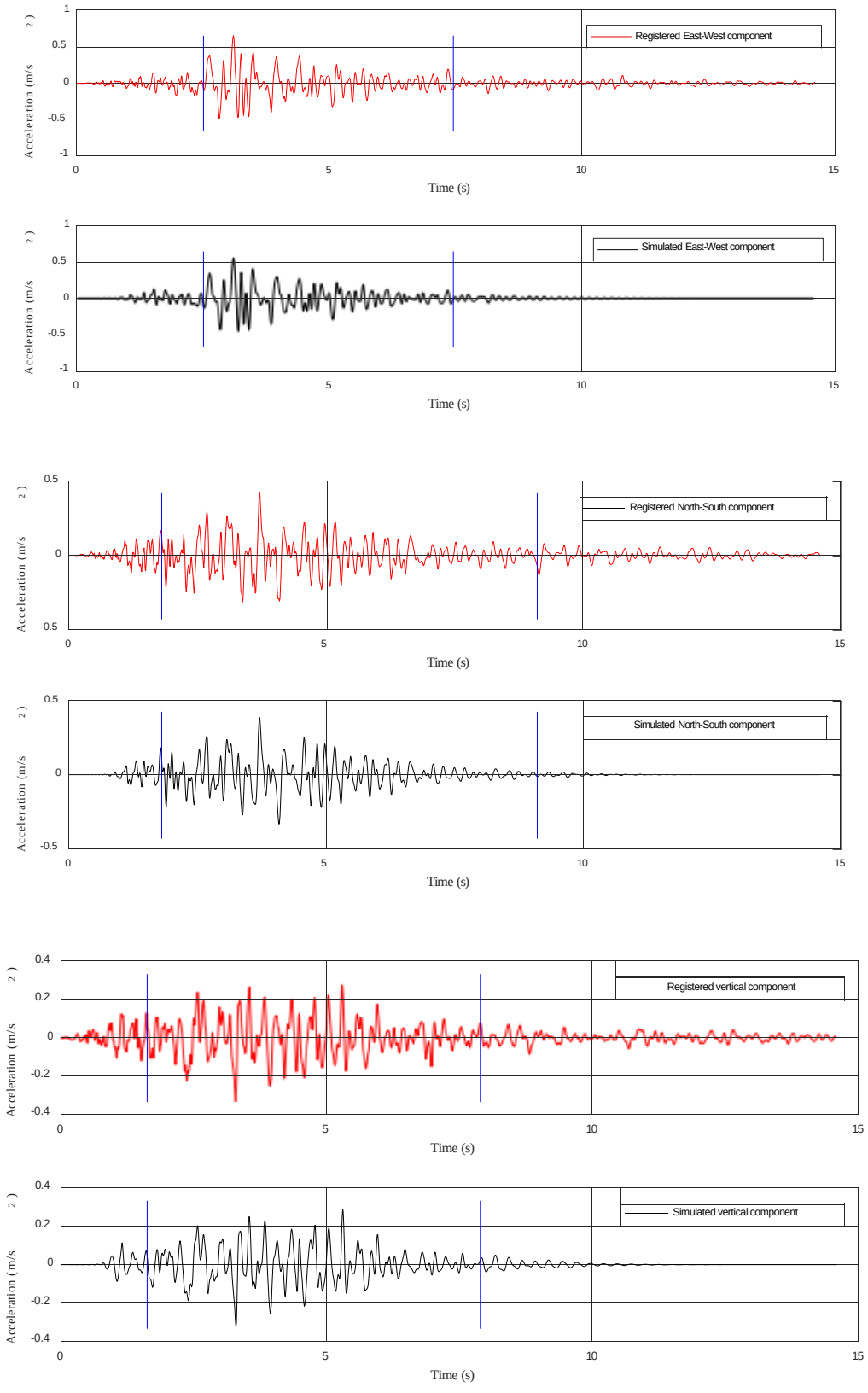


**Figure 3.** Components of the accelerograms Registered (above) and Simulated (below) at the Piedimonte Matese station,using the imaginary part of the Morlet's wavelets.

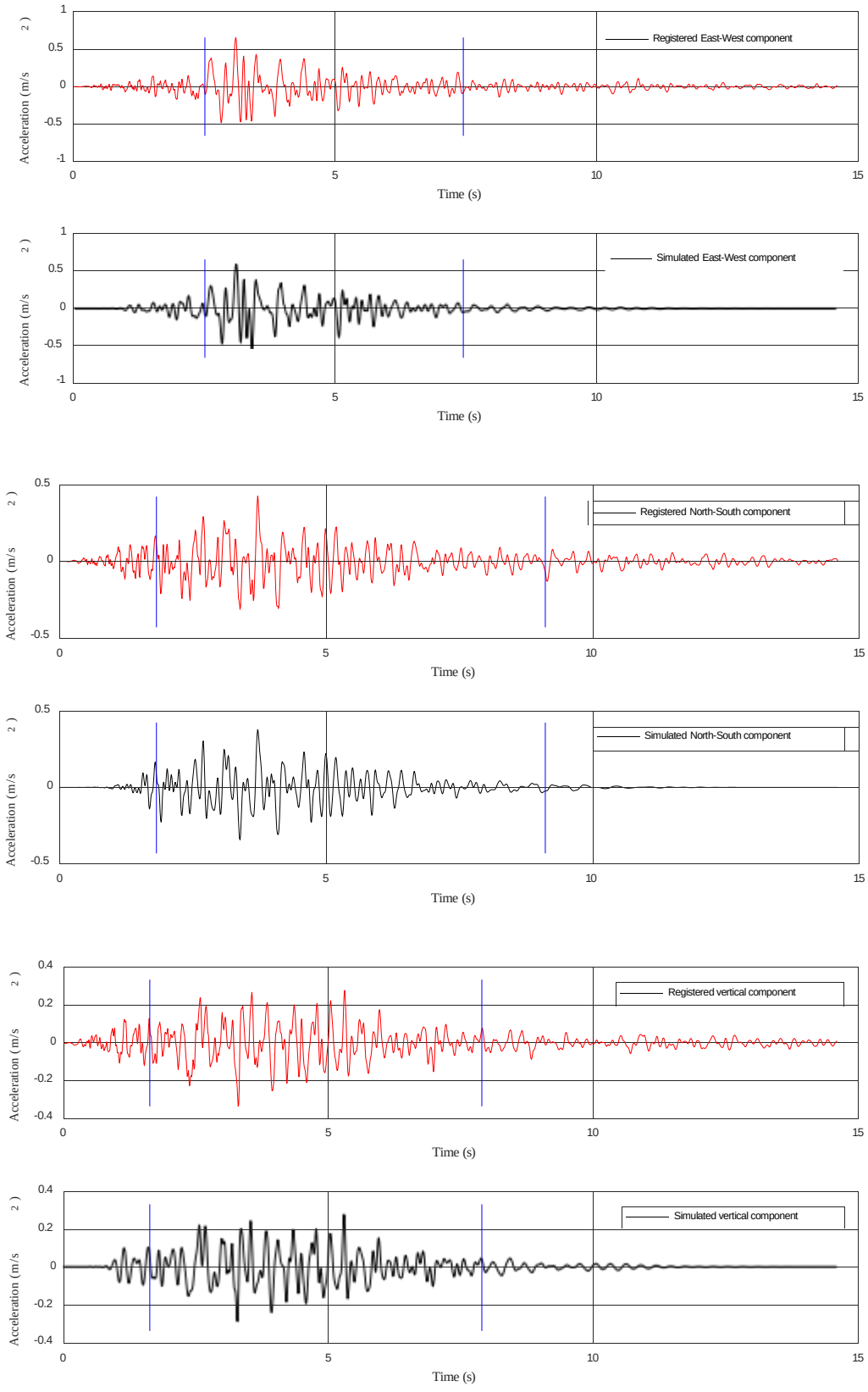


**Figure 4.** Components of the accelerograms Registered (above) and Simulated (below) at the Piedimonte Matese station,using the real part of the Morlet's wavelets.

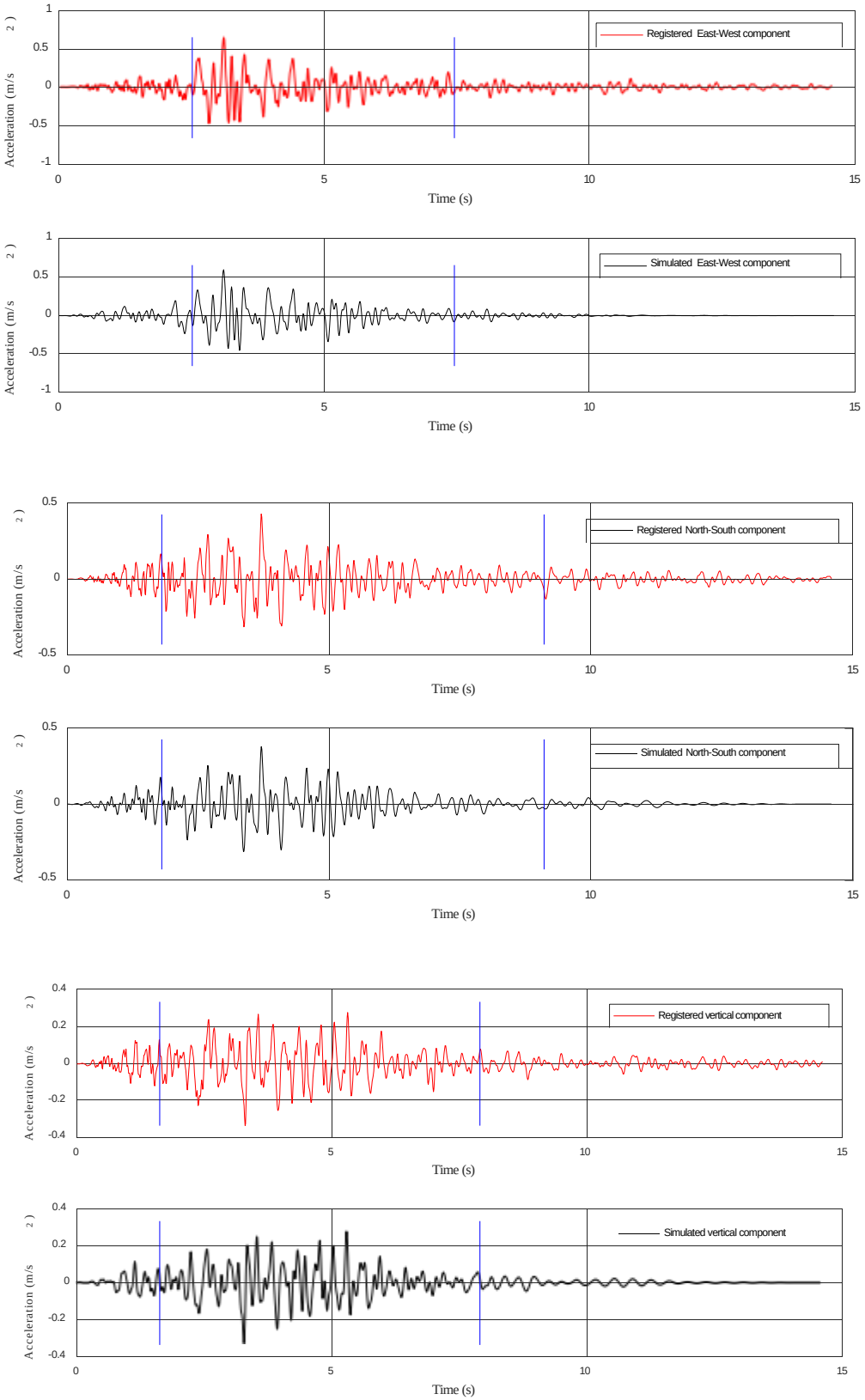


**Figure 5.** Components of the accelerograms Registered (above) and Simulated (below) at the Piedimonte Matese station, using the Bruna and Riera [9] function.

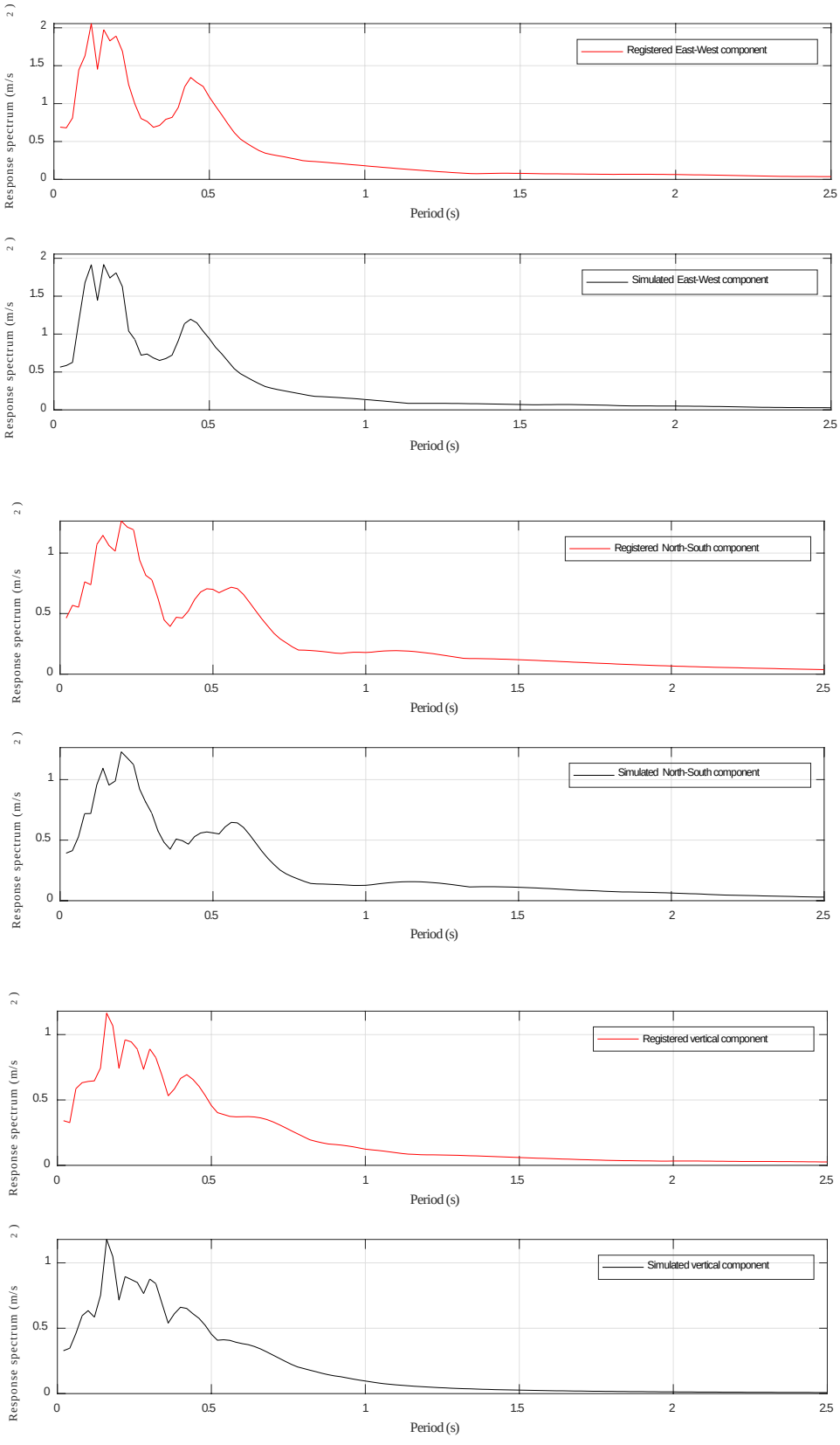


**Figure 6.** Components of the pseudo-acceleration spectra Registered (above) and Simulated (below) at the Piedimonte Matese station, using the imaginary part of the Morlet's wavelets.

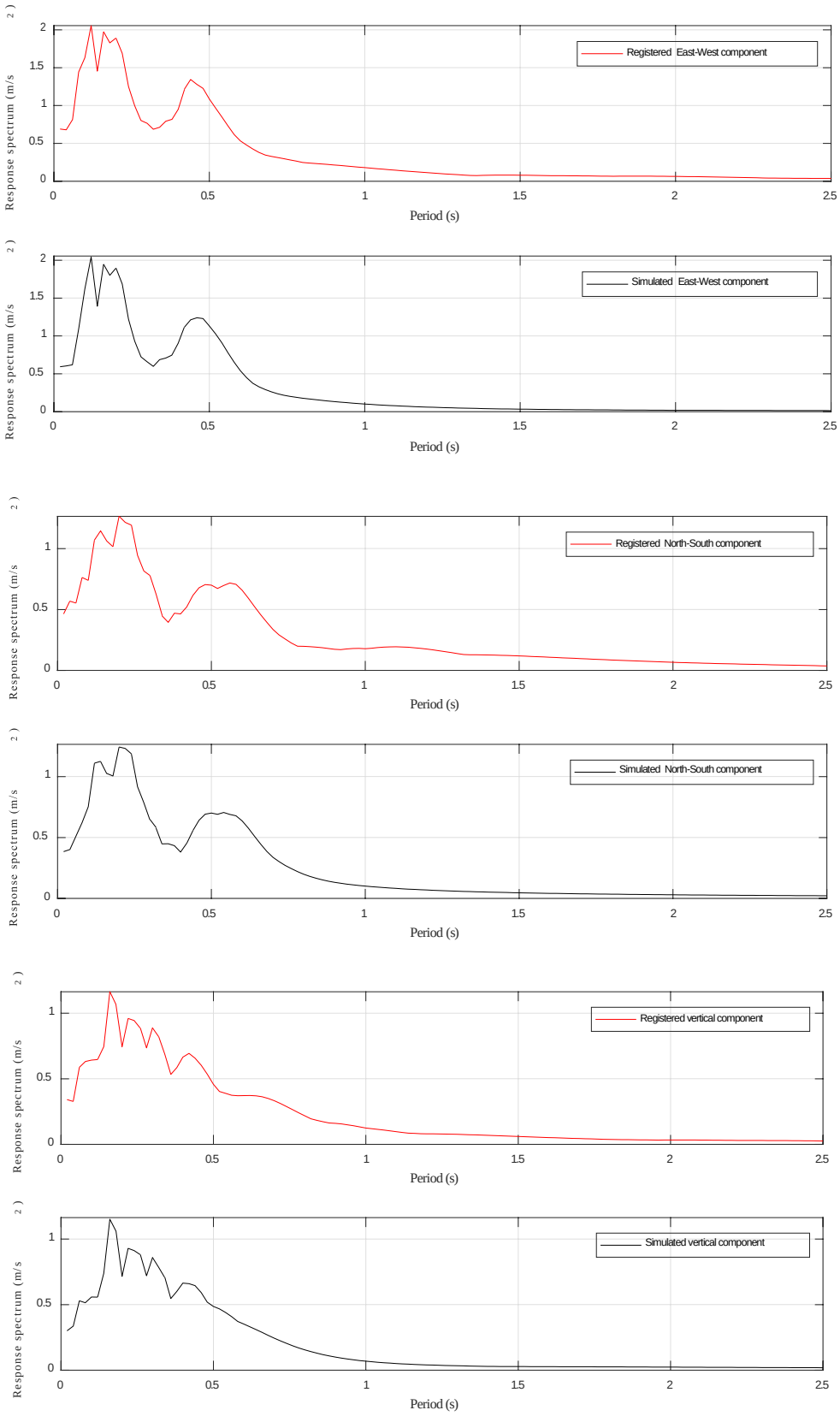


**Figure 7.** Components of the pseudo-acceleration spectra Registered (above) and Simulated (below) at the Piedimonte Matese station, using the real part of the Morlet's wavelets.

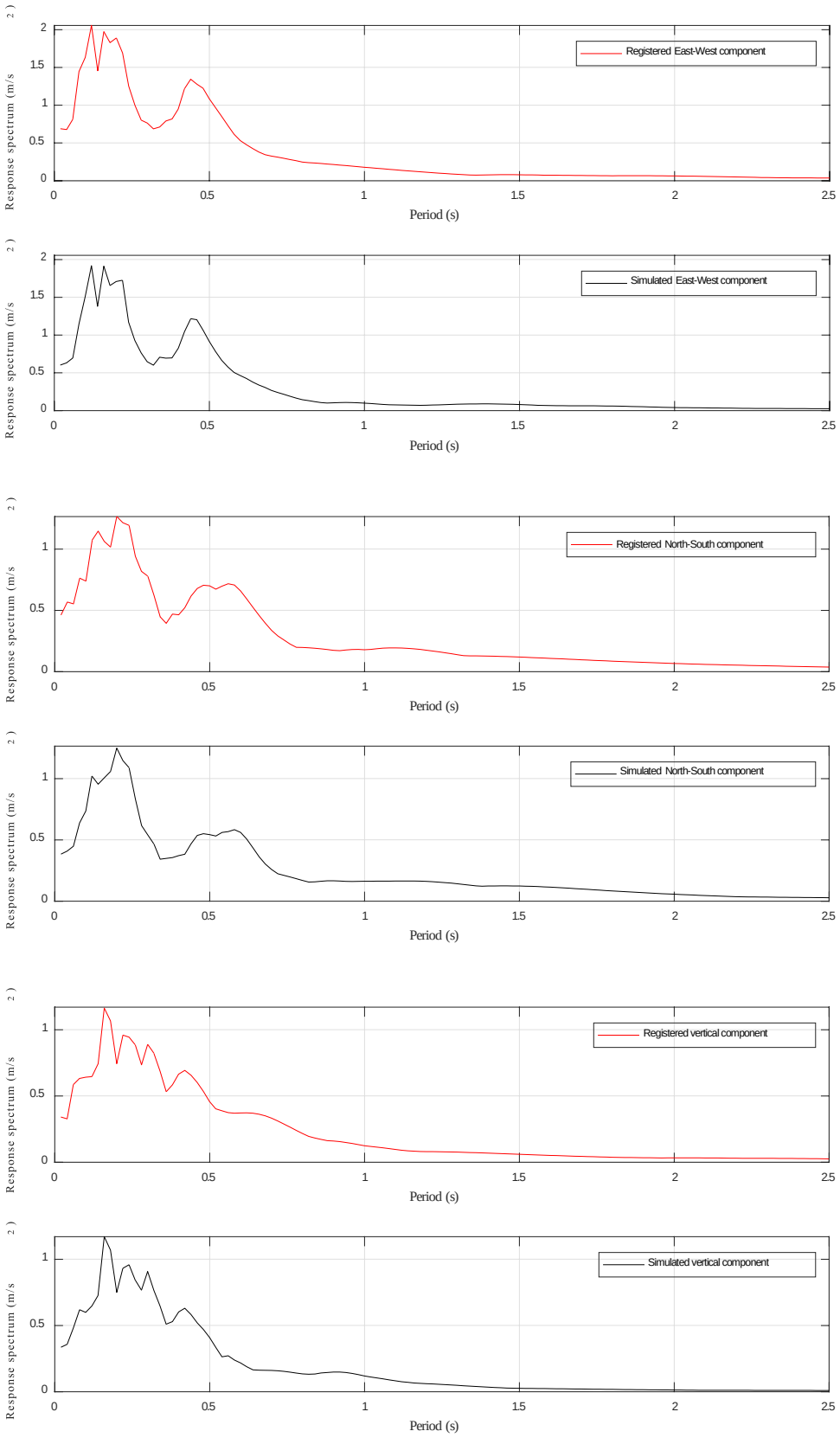


**Figure 8.** Components of the pseudo-acceleration spectra Registered (above) and Simulated (below) at the Piedimonte Matese station, using the Bruna and Riera [9] function.

**Table 2.** Mean-squared error of pseudo-acceleration spectra (difference between registered and simulated spectra in $m^2/s^4$) at PDM station, for the period from 0 s to 2.5 s.

| Component (function) | Morlet (imaginary part) | Morlet (real part) | Bruna and Riera [9] |
|---|---|---|---|
| EW | 0.0037 | 0.0042 | 0.0058 |
| NS | 0.0019 | 0.0035 | 0.0044 |
| Vertical | 0.0009 | 0.0015 | 0.0034 |
| Mean | 0.0022 | 0.0031 | 0.0045 |

**Table 3.** Relative error of the peak of the pseudo-acceleration spectra (difference between registered and simulated peaks) at PDM station.

| Component (function) | Morlet (imaginary part) | Morlet (real part) | Bruna and Riera [9] |
|---|---|---|---|
| EW | 0.0671 | 0.0670 | 0.0675 |
| NS | 0.0277 | 0.0177 | 0.0125 |
| Vertical | 0.0135 | 0.0107 | 0.0059 |
| Mean | 0.0361 | 0.0318 | 0.0286 |

**Table 4.** Mean-squared error of the accelerograms (difference between registered and simulated accelerograms in $m^2/s^4$) at the PDM station.

| Component (function) | Morlet (imaginary part) | Morlet (real part) | Bruna and Riera [9] |
|---|---|---|---|
| EW | 0.0014 | 0.0014 | 0.0016 |
| NS | 0.0009 | 0.0010 | 0.0010 |
| Vertical | 0.0006 | 0.0006 | 0.0006 |
| Mean | 0.0010 | 0.0010 | 0.0011 |

**Table 5.** Relative error of the peak ground accelerations (difference between registered and simulated peaks), at the PDM station.

| Component (function) | Morlet (imaginary part) | Morlet (real part) | Bruna and Riera [9] |
|---|---|---|---|
| EW | 0.1475 | 0.1009 | 0.0913 |
| NS | 0.0955 | 0.1154 | 0.1171 |
| Vertical | 0.0315 | 0.1256 | 0.0106 |
| Mean | 0.0915 | 0.1140 | 0.0730 |

**Table 6.** Final velocity according to simulated accelerograms at the PDM station (m/s).

| Component (function) | Morlet (imaginary part) | Morlet (real part) | Bruna and Riera [9] |
|---|---|---|---|
| EW | 0.00 | 0.00 | 0.00 |
| NS | 0.00 | 0.01 | 0.00 |
| Vertical | 0.00 | 0.01 | 0.00 |
| Mean | 0.00 | 0.01 | 0.00 |

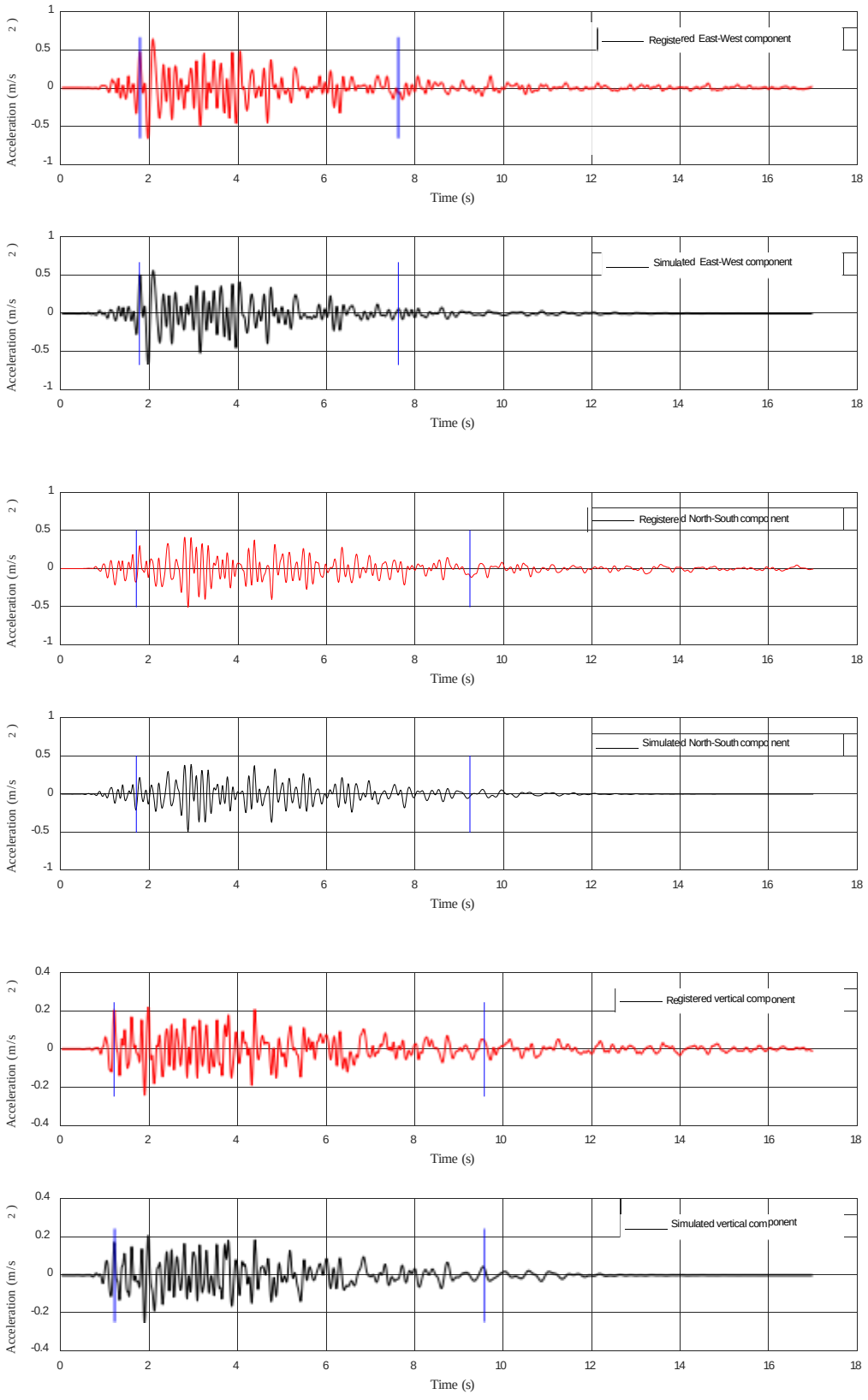


**Figure 9.** Three components of the accelerograms Registered (above) and Simulated (below) at the Cairano 4 station, using the imaginary part of the Morlet's wavelets.

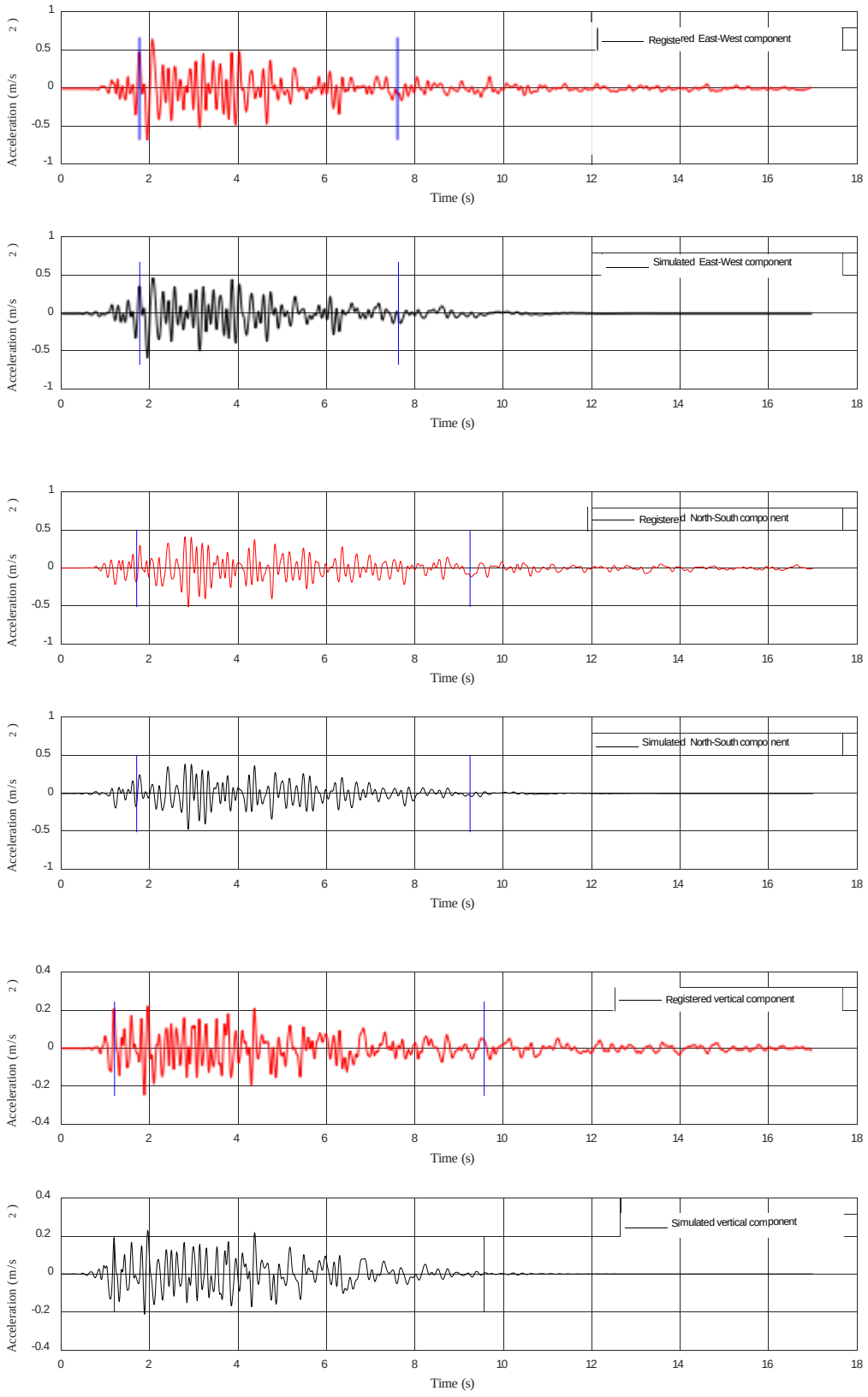


**Figure 10.** Three components of the accelerograms Registered (above) and Simulated (below) at the Cairano 4 station, using the real part of the Morlet's wavelets.

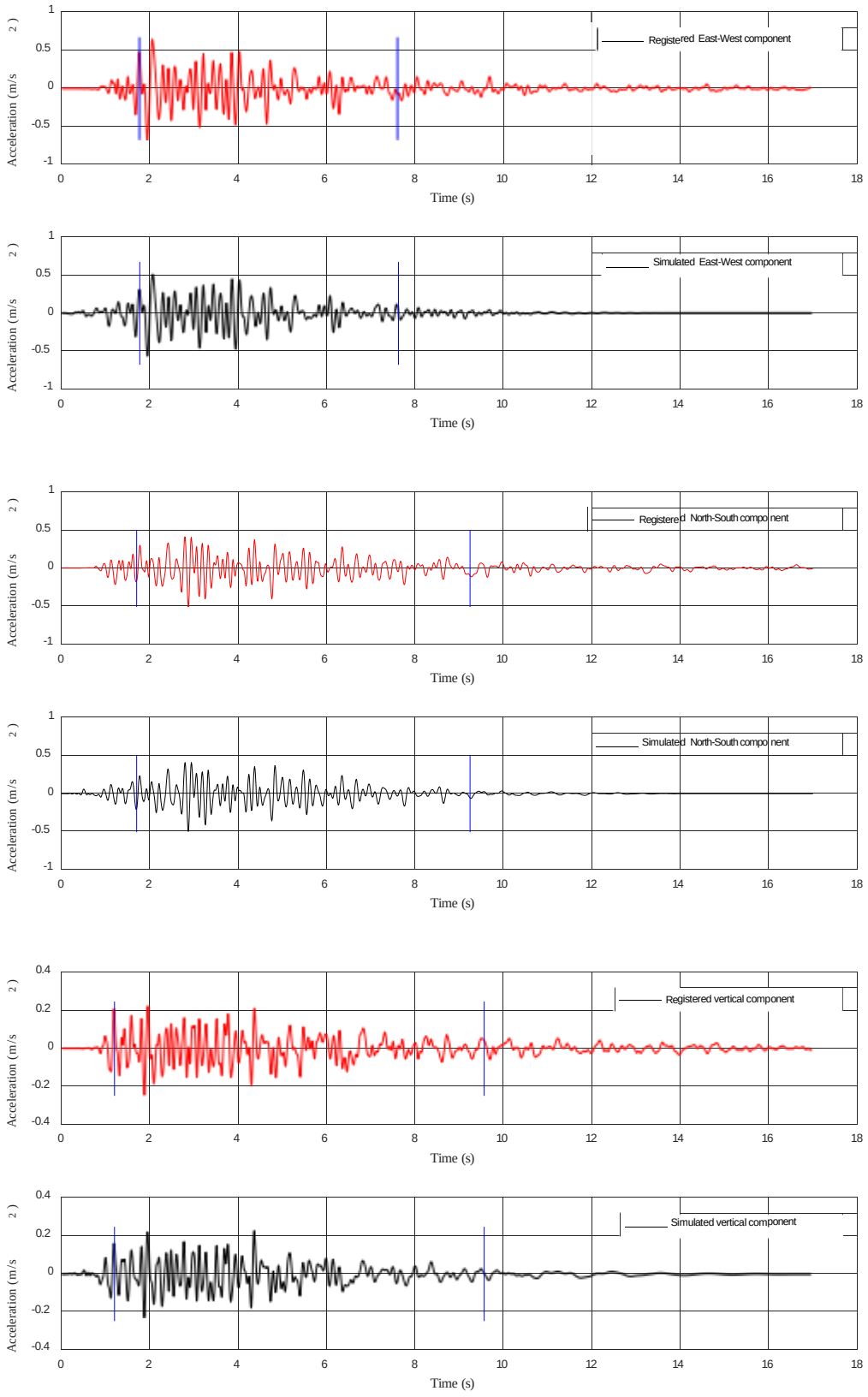


**Figure 11.** Three components of the accelerograms Registered (above) and Simulated (below) at the Cairano 4 station, using the Bruna and Riera [9] function.

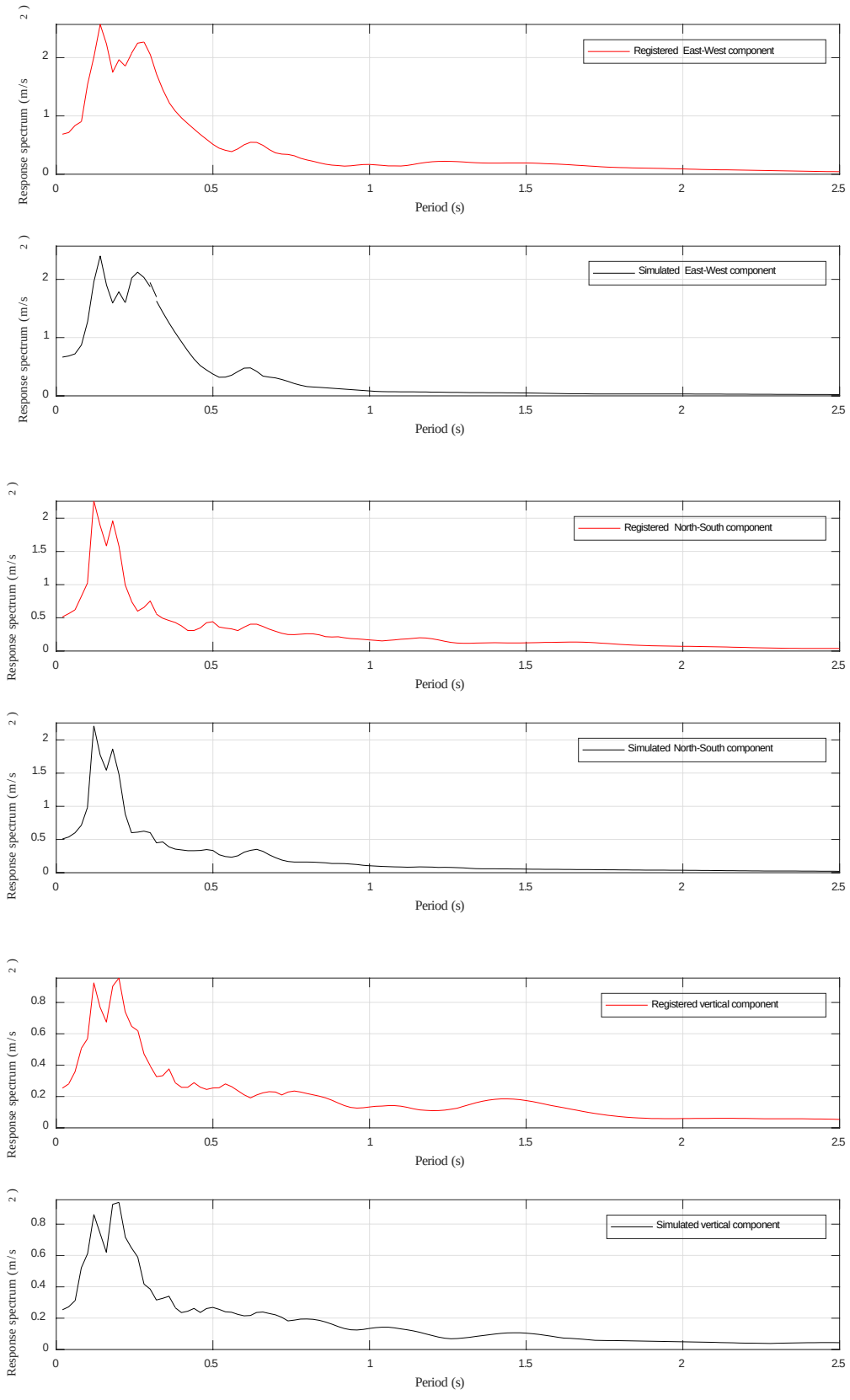


**Figure 12.** Three components of the pseudo-acceleration spectra Registered (above) and Simulated (below) at the Cairano 4 station,using the imaginary part of the Morlet's wavelets.

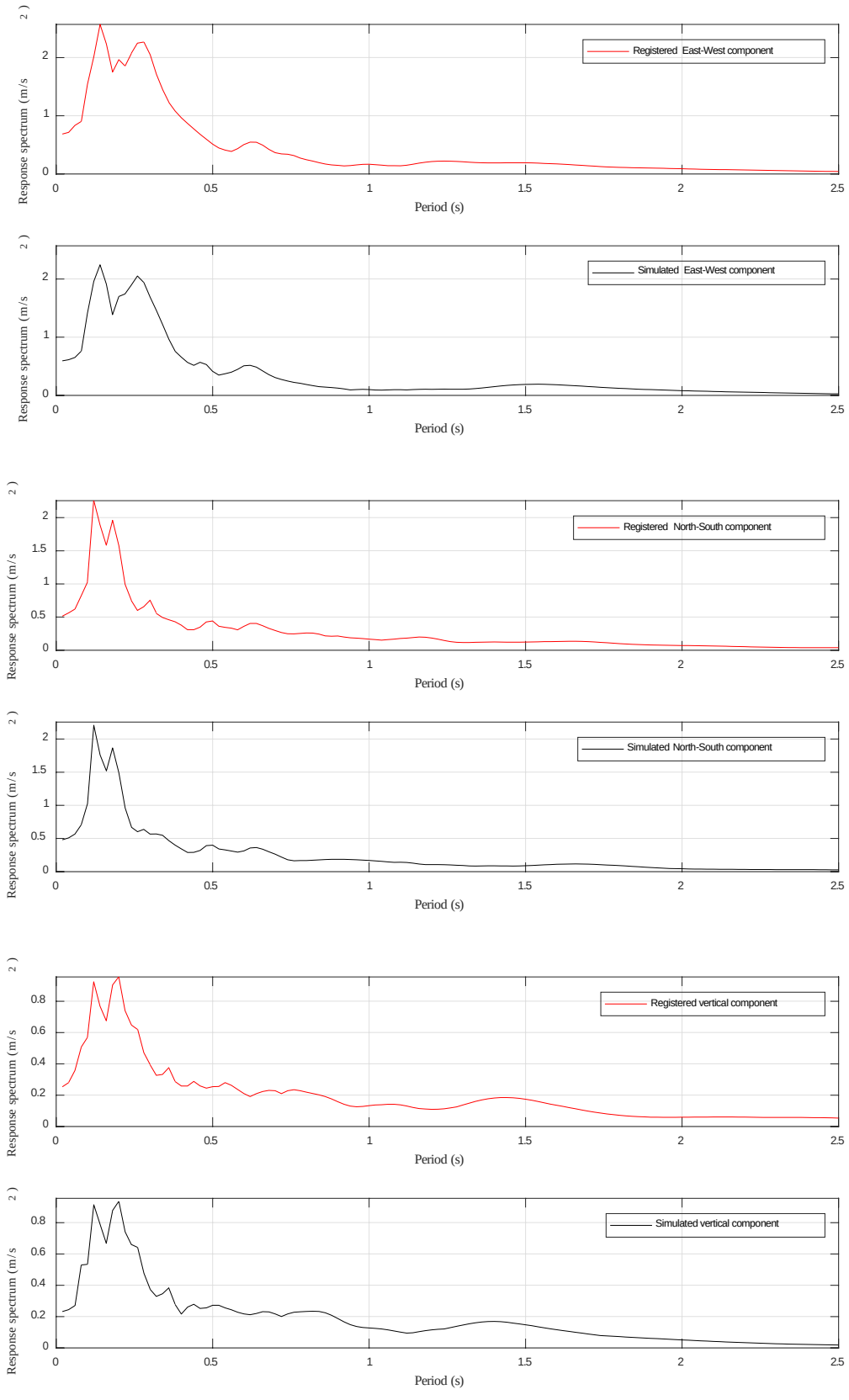


**Figure 13.** Three components of the pseudo-acceleration spectra Registered (above) and Simulated (below) at the Cairano 4 station,using the real part of the Morlet's wavelets.

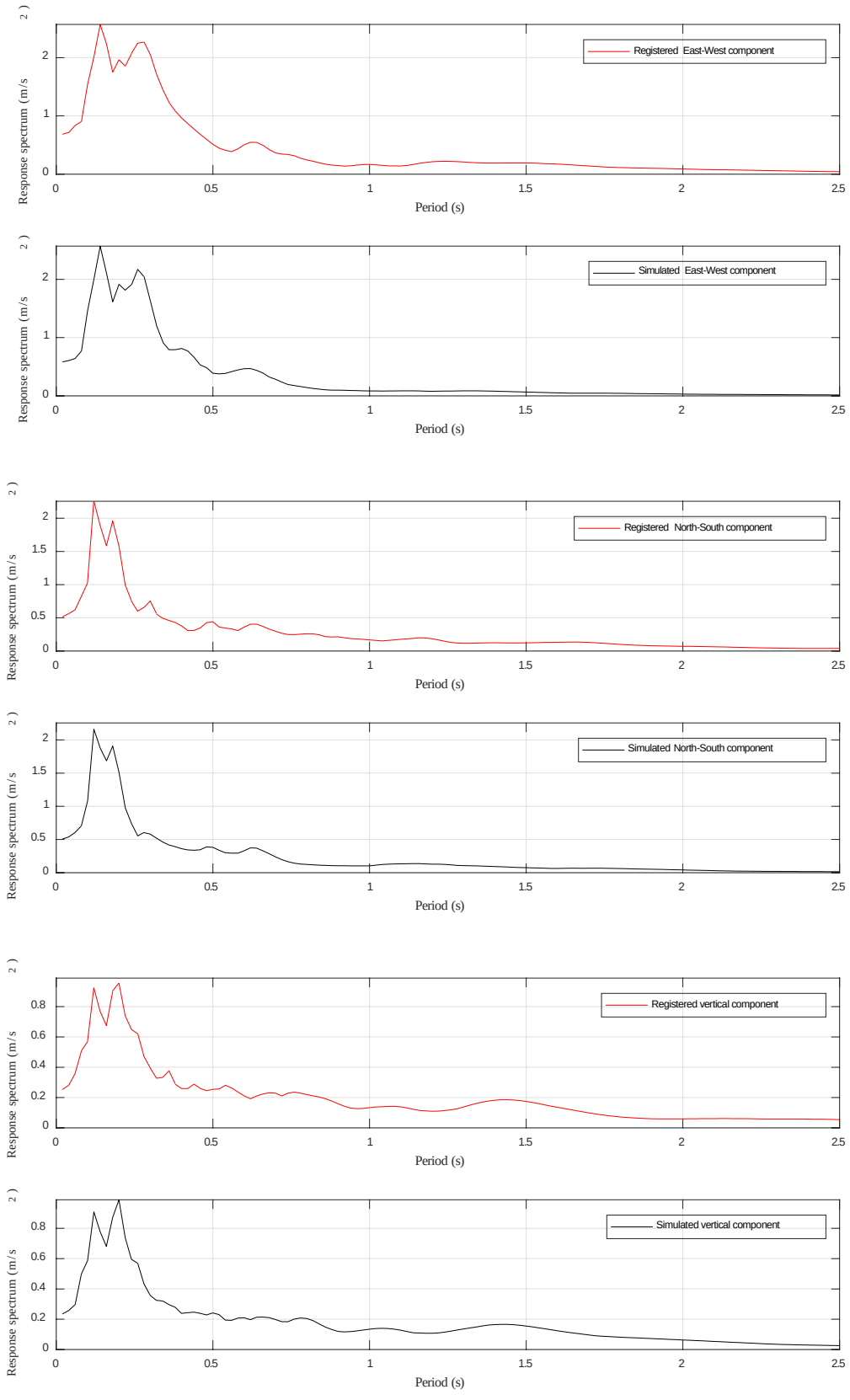


**Figure 14.** Three components of the pseudo-acceleration spectra Registered (above) and Simulated (below) at the Cairano 4 station, using the Bruna and Riera [9] function.

### 4.2 Cairano 4 Station (1981)

Figures 9-14 present the results of the three components with respect to the earthquake recorded at the CR4 station. Figures 9-11 illustrate the registered accelerograms and the simulated accelerograms and Figures 12-14 illustrate the registered and simulated pseudo-acceleration spectra. The vertical bars (in blue) of Figures 9-11 indicate the duration of the strong motion, calculated by the method proposed by Trifunac and Brady [30].

Tables 7-11 show results for the CR4 station. Table 7 shows the mean-squared error among the pseudo-acceleration spectra, for the period from 0 s to 2.5 s. Table 8 shows the relative error among the peak pseudo-acceleration spectra. Table 9 shows the mean-squared error among the accelerograms. Table 10 shows the relative error among the peak ground acceleration. Table 11 shows the final velocity of the simulated accelerograms.

**Table 7.** Mean-squared error of the pseudo-acceleration spectra (difference between registered and simulated spectra in $m^2/s^4$) at the CR4 station, for the period from 0 s to 2.5 s.

| Component (function) | Morlet (imaginary part) | Morlet (real part) | Bruna and Riera [9] |
|---|---|---|---|
| EW | 0.0115 | 0.0131 | 0.0163 |
| NS | 0.0046 | 0.0019 | 0.0031 |
| Vertical | 0.0012 | 0.0005 | 0.0006 |
| Mean | 0.0058 | 0.0052 | 0.0067 |

**Table 8.** Relative error of the peak of the pseudo-acceleration spectra (difference between registered and simulated peaks) at the CR4 station.

| Component (function) | Morlet (imaginary part) | Morlet (real part) | Bruna and Riera [9] |
|---|---|---|---|
| EW | 0.0666 | 0.1272 | 0.0012 |
| NS | 0.0208 | 0.0217 | 0.0423 |
| Vertical | 0.0176 | 0.0213 | 0.0346 |
| Mean | 0.0350 | 0.0567 | 0.0260 |

**Table 9.** Mean-squared error of the accelerograms (difference between registered and simulated accelerograms in $m^2/s^4$) at the CR4 station.

| Component (function) | Morlet (imaginary part) | Morlet (real part) | Bruna and Riera [9] |
|---|---|---|---|
| EW | 0.0016 | 0.0015 | 0.0017 |
| NS | 0.0011 | 0.0012 | 0.0010 |
| Vertical | 0.0004 | 0.0003 | 0.0004 |
| Mean | 0.0010 | 0.0010 | 0.0010 |

**Table 10.** Relative error of the peak ground accelerations (difference between registered and simulated peaks), at the CR4 station.

| Component (function) | Morlet (imaginary part) | Morlet (real part) | Bruna and Riera [9] |
|---|---|---|---|
| EW | 0.0278 | 0.1295 | 0.1451 |
| NS | 0.0194 | 0.0682 | 0.0215 |
| Vertical | 0.0017 | 0.0772 | 0.0703 |
| Mean | 0.0163 | 0.0916 | 0.0790 |

**Table 11.** Final velocity according to simulated accelerograms at the CR4 station (m/s).

| Component (function) | Morlet (imaginary part) | Morlet (real part) | Bruna and Riera [9] |
|---|---|---|---|
| EW | 0.00 | 0.00 | 0.00 |
| NS | 0.00 | 0.00 | 0.00 |
| Vertical | 0.00 | 0.00 | 0.00 |
| Mean | 0.00 | 0.00 | 0.00 |

## 5. Waveform Performance in Seismic Motion Simulation

Visual comparisons of recorded and simulated accelerograms and corresponding pseudo-acceleration spectra reveal a very close agreement in all cases. All features of both the acceleration records and associated spectra, considered relevant in engineering analysis and design, are correctly modeled by the proposed procedure and model assumptions, for the three wave functions herein examined. These include the evolution with time of the frequency content of the acceleration records, the total duration,the rms and peak values of both the acceleration records and the corresponding spectra.

Observed errors are small and no specific trend was detected in the events examined. For instance, in the case of PDM Station, the mean-squared error for the spectral values in the range between 0 s and 2.5 s (mean of the three components) is 0.0022 $m^2/s^4$, 0.0031 $m^2/s^4$ and 0.0045 $m^2/s^4$ for the imaginary and real parts of Morlet's wavelets and Bruna and Riera [9] function, respectively. For the event registered at CR4 Station, those values were 0.0058 $m^2/s^4$, 0.0052 $m^2/s^4$ and 0.0067 $m^2/s^4$, respectively. The relative errors between simulated and observed peak values of the spectra were larger, but the smallest values are not associated with the same waveform type.

Although the database is certainly insufficient to establish a robust assessment, it is concluded that the mean-squared error of simulated spectra for the three waveform functions and the two stations examined are of the order of 0.005 $m^2/s^4$, while relative errors in peak values vary around 4%. Similar analyzes showed that the mean-

squared error between simulated and registered acceleration time-histories for the three waveform functions and the two stations examined are 0.001 $m^2/s^4$, while relative errors in peak values vary around 7.7%.

Finally, it was previously remarked that the imaginary part of Morlet's wavelets and Bruna and Riera [9] function has zero integrals, consequently the sum of any number of terms will also have a null area. The condition of zero final velocity, which should be satisfied by any seismic acceleration record, is thus automatically satisfied by the imaginary part of Morlet's wavelets and Bruna and Riera [9] function, but not by the real part of Morlet's wavelets (See Tables 6 and 11). The error of the latter is small in the cases studied, but may be important in the simulation of short duration, impulsive earthquakes.

## 6. Conclusions

The performance of a numerical procedure, based on an evolutionary optimization algorithm, for the simultaneous generation of the three components of the seismic ground acceleration caused by the incidence of body waves, was proposed and examined in the paper for three different waveforms types, namely, the imaginary and real parts of Morlet's wavelets,and Bruna and Riera function. All three types result in accelerograms and corresponding spectra that closely resemble recorded graphs, with mean-squared errors of the order of 0.005 $m^2/s^4$ and minor differences between the errors of the evaluated options. The imaginary part of Morlet's wavelets, and Bruna and Riera function have the advantage that the simulated three components of the final ground velocity would always be identically zero. Knowing the waves that generate these three seismic components at one location (seismic station), these same seismic waves may be used for the simulation of the three seismic acceleration time-histories at other locations on the surface in the vicinity of the seismic station, thus improving seismic analysis and design of large structures, such as long-span bridges, transmission lines, dams or retaining structures, in which the assumption that the ground accelerations throughout the entire contact surface between the structure and the ground are fully correlated may lead to large response prediction errors.

## Data and Resources

Accelerograms can be obtained from the Engineering Strong-Motion database at https://esm.mi.ingv.it (last accessed April 2021).

## Conflict of Interest

There is no conflict of interest.

## Acknowledgments

The authors acknowledge the financial support of *Conselho Nacional de Desenvolvimento Científico e Tecnológico* (CNPq) and *Coordenação de Aperfeiçoamento de Pessoal deNível Superior* (CAPES).

## References

[1] Housner, G.W., 1947. Characteristics of strong-motion earthquakes. Bulletin of the Seismological Society of America. 37(1), 19-31.
DOI: https://doi.org/10.1785/BSSA0370010019

[2] Bycroft, G.N., 1960. White noise representation of earthquakes. Journal of the Engineering Mechanics Division (ASCE). 86, 1-16.
DOI: https://doi.org/10.1061/JMCEA3.0000125

[3] Tajimi, H., 1960. A statistical method of determining the maximum response of a building structure during an earthquake. In: Proceedings of 2th World Conference in Earthquake Engineering, Tokyo, Japan. 1, 781-797.

[4] Kanai, K., 1961. An empirical formula for the spectrum of strong earthquake motions. Bulletin Earthquake Research Institute. (39), 85-95.

[5] Clough, R., Penzien, J., 1993. Dynamics of Structures. McGraw-Hill, Inc.

[6] Shinozuka, M., Sato, Y., 1967. Simulation of nonstationary random process. Journal of Engineering Mechanics (ASCE). 93, 11-40.
DOI: https://doi.org/10.1061/JMCEA3.0000822

[7] Iyengar, R.N., Iyengar, K.T.S., 1969. Anonstationary random process model for earthquake acceleration. Bulletin of the Seismological Society of America. 59(3), 1163-1188.
DOI: https://doi.org/10.1785/BSSA0590031163

[8] Amin, M., Ang, A.H.S., 1968. Non-stationary stochastic model of earthquake motion. Journal of Engineering Mechanics (ASCE). 94, 559-583.
DOI: https://doi.org/10.1061/JMCEA3.0000969

[9] Bruna, R.A., Riera, J.D., 1988. Towards the simultaneous generation of the three components of the seismic acceleration on rock surface. Nuclear Engineering & Design. 110(2), 153-163.
DOI: https://doi.org/10.1016/0029-5493(88)90017-9

[10] Dalla Chiesa, D., Miguel, L.F.F., 2019. Methodology for simulation of the three components of seismic acceleration. Bulletin of the Seismological Society of America. 109(6), 2427-2436.
DOI: https://doi.org/10.1785/0120190042

[11] Dalla Chiesa, D., Miguel, L.F.F., Riera, J.D., 2021. Simultaneous simulation of the three components of

seismic accelerograms at locations around seismological stations. Journal of Seismology. 25, 1361-1384.
DOI: https://doi.org/10.1007/s10950-021-10050-z

[12] Iturrioz, I., Riera, J.D., 2021. Assessment of the Lattice Discrete Element Method in the simulation of wave propagation in inhomogeneous linearly elastic geologic materials. Soil Dynamics and Earthquake Engineering. 151, 106952.
DOI: https://doi.org/10.1016/j.soildyn.2021.106952

[13] Spanos, P.D., Giaralis, A., Politis, N.P., 2007. Numerical Treatment of Seismic accelerograms and of Inelastic Seismic Structural Responses Using Harmonic Wavelets. Computer-Aided Civil and Infrastructure Engineering. 22, 254-264.
DOI: https://doi.org/10.1111/j.1467-8667.2007.00483.x

[14] Newland, D.E., 1994a. Wavelet analysis of vibration, Part I: Theory. Journal of Vibrations and Acoustics. 116(4), 409-416.
DOI: https://doi.org/10.1115/1.2930443

[15] Newland, D.E., 1994b. Wavelet analysis of vibration, Part II: Wavelet maps. Journal of Vibrations and Acoustics. 116(4), 417-425.
DOI: https://doi.org/10.1115/1.2930444

[16] Newland, D.E., 1999. Ridge and phase identification in the frequency analysis of transient signals by harmonic wavelets. Journal of Vibrations and Acoustics. 121(2), 149-155. DOI: https://doi.org/10.1115/1.2893957

[17] Gurley, K., Kareem, A., 1999. Applications of wavelet transforms in earthquake, wind and ocean engineering. Engineering Structures. 21, 149-167.
DOI: https://doi.org/10.1016/S0141-0296(97)00139-9

[18] Montejo, L.A., Suárez, L.E., 2006. Wavelet-based identification of site frequencies from earthquake records. Journal of Earthquake Engineering. 10(4), 565-594.
DOI: https://doi.org/10.1080/13632460609350610

[19] Amiri, G.G., Shahjouei, A., Saadat, S., et al., 2011. Hybrid Evolutionary-Neural Network Approach in Generation of Artificial Accelerograms Using Principal Component Analysis and Wavelet-Packet Transform. Journal of Earthquake Engineering. 15(1), 50-76.
DOI: https://doi.org/10.1080/13632469.2010.517281

[20] Yamamoto, Y., Baker, J.W., 2013. Stochastic Model for Earthquake Ground Motion Using Wavelet Packets. Bulletin of the Seismological Society of America. 103(6), 3044-3056.
DOI: https://doi.org/10.1785/0120120312

[21] Domingues, M.O., Mendes, O., Kaibara, M.K., et al., 2016. Explorando a transformada wavelet contínua. Revista Brasileira de Ensino de Física. 38.
DOI: https://doi.org/10.1590/1806-9126-RBEF-2016-0019

[22] Civicioglu, P., 2013. Backtracking search optimization algorithm for numerical optimization problems. Applied Mathematics and Computation. 219(15), 8121-8144.
DOI: https://doi.org/10.1016/j.amc.2013.02.017

[23] Miguel, L.F.F., Miguel, L.F.F., Lopez, R.H., 2016a. Simultaneous optimization of force and placement of friction dampers under seismic loading. Engineering Optimization. 48(4), 582-602.
DOI: https://doi.org/10.1080/0305215X.2015.1025774

[24] Miguel, L.F.F., Miguel, L.F.F., Lopez, R.H., 2016b. Failure probability minimization of buildings through passive friction dampers. Structural Design of Tall and Spectral Buildings. 25(17), 869-885.
DOI: https://doi.org/10.1002/tal.1287

[25] Kennett, B.L.N., Engdahl, E.R., 1991. Travel times for global earthquake location and phase association. Geophysical Journal International. 105, 429-465. http://ds.iris.edu/spud/earthmodel/10131355.

[26] Bollettino Sismico Italiano - Istituto Nazionale di Geofisica e Vulcanologia, Centro Nazionale Terremoti. http://bollettinosismico.rm.ingv.it/.

[27] Castello, B., Selvaggi, G., Chiarabba, C., et al., 2006. CSI Catalogo della sismicità italiana 1981-2002, versione 1.1. INGV-CNT, Roma. http://www.ingv.it/CSI/.

[28] ESM - Engineering Strong-Motion database. (accessed April 2021). https://esm.mi.ingv.it

[29] Luzi, L., Lanzano, G., Felicetta, C., et al., 2020. Engineering Strong Motion Database (ESM) (Version 2.0). Istituto Nazionale di Geofisica e Vulcanologia (INGV).
DOI: https://doi.org/10.13127/ESM.2

[30] Trifunac, M.D., Brady, A.G., 1975. A Study of the duration of strong earthquake ground motion. Bulletin of the Seismological Society of America. 65(3), 581-626.
DOI: https://doi.org/10.1785/BSSA0650030581